

## Supporting Information

### **Plasmonic Cu-Ni bimetal nanoparticles coupled with ultrathin CdS nanosheet for remarkably improved photocatalytic H<sub>2</sub> generation under visible-light irradiation**

Qingru Zeng,<sup>a</sup> Yining Bao,<sup>b</sup> Shunyan Ning,<sup>a</sup> Qingguo Yu,<sup>b</sup> Yuezhou Wei<sup>a</sup> and Deqian Zeng<sup>\*a</sup>

<sup>a</sup> School of Nuclear Science and Technology, University of South China, Hengyang, 421001, China

<sup>b</sup> School of Resources, Environment and Materials, Guangxi University, Nanning 530004, China

\*Corresponding author. Email: dqzeng@usc.edu.cn (D. Zeng)

# Contents

Supporting Information.....	1
Contents .....	2
Chemicals.....	4
Characterization.....	4
Photocatalytic measurements.....	5
Photoelectrochemical measurements .....	5
Density functional theory calculations.....	6
Fig. S1.....	7
Fig. S2.....	8
Fig. S3.....	9
Fig. S4.....	10
Fig. S5.....	11
Fig. S6.....	12
Fig. S7.....	13
Fig. S8.....	14
Fig. S9.....	15
Fig. S10.....	16
Fig. S11 .....	17
Fig. S12.....	18
Fig. S13.....	19
Fig. S14.....	20
Fig. S15.....	21
Fig. S16.....	22
Fig. S17.....	23
Fig. S18.....	24
Fig. S19.....	25

Fig. S20.....	26
Fig. S21.....	27
Fig. S22.....	28
Fig. S23.....	29
Fig. S24.....	30
Fig. S25.....	31
Fig. S26.....	32
Fig. S27.....	33
Table S1 .....	34
Table S2 .....	35
Table S3 .....	36
Table S4 .....	37
Table S5 .....	38
References.....	39

## **Chemicals**

Oleylamine, nickel acetylacetonate, copper acetylacetonate, thiourea were purchased from J&K Scientific Ltd. Benzyl alcohol was obtained from Tianjin Kermel Ltd. Dibenzyl ether and 1-hexadecanol were purchased from Sigma-Aldrich. Trioctylphosphine oxide was obtained from Strem chemicals. Ethylenediamine was purchased from Sinopharm Chemical Reagent Co., Ltd. Cadmium acetate dihydrate was obtained from Thermo Fisher Scientific Inc. All chemicals and reagents were used without further purification. Deionized (DI) water was used throughout the whole experiment.

## **Characterization**

The crystallinity and structure were performed on a Rigaku D/MAX 2500V X-ray diffraction (XRD) diffractometer (Rigaku Ltd., Japan). Morphologies and microstructures were acquired by a scanning electron microscopy (SEM, ZEISS Sigma 360) and a field emission transmission electron microscope (TEM, Thermo Talos F200X G2). Ultraviolet-visible (UV-Vis) spectra were carried out using a UV-Vis spectrometer (UV-3600Plus). XPS analysis were performed by a Thermo Escalab 250 X-ray photoelectron spectroscopy with a monochromatic Al K $\alpha$  X-ray source. Photoluminescence (PL) spectra were acquired using an OmniFluo990LSP fluorescence spectrometer. Time-resolved photoluminescence (TRPL) spectra were measured on the FL3C-111 TCSPC fluorescence spectrometer. The Brunauer-Emmett-Teller (BET) surface area and pore structures were analyzed using N<sub>2</sub> adsorption-desorption experiments on a Micro-meritics instrument TriStar. The surface photovoltage (SPV) of the samples was investigated using a surface photovoltage system (CEL-SPS1000). The concentration of Cu, Ni, and Cd was

measured on an inductively coupled plasma-optical emission spectrometer (ICP-OES, ULTIMA Expert LT).

### **Photocatalytic measurements**

Photocatalytic H<sub>2</sub> production reactions were performed in a sealed Pyrex flask reaction of photocatalytic activity evolution system. In a typical procedure, 30 mg of as-prepared sample powders were evenly dispersed into 60 ml Na<sub>2</sub>S (0.35 M) and Na<sub>2</sub>SO<sub>3</sub> (0.25 M) aqueous solution. The temperature of the system was maintained at 6 °C by circulating water system. The mixed aqueous solution of Na<sub>2</sub>S and Na<sub>2</sub>SO<sub>3</sub> serves as a sacrificial agent to consume photoinduced holes. The whole suspension was evacuated to remove the dissolved air prior to light irradiation. Visible Light was generated by a 300 W Xenon lamp (Aulight) coupled with a 420 nm UV cut-off filter . Photons at a particular wavelength was generated by filtering the output with different band pass filter ( $\lambda=400, 420, 435, 450, 475, 500, 520, 550, 600, 650, 700$  nm). The apparent quantum yield (AQY) was calculated using the following equation:

$$\text{AQY}(\%) = \frac{\text{number of evolved H}_2 \text{ molecules} \times 2}{\text{number of incident photons}} \times 100\%$$

### **Photoelectrochemical measurements**

All photoelectrochemical (PEC) measurements were tested in a three-electrode configuration on a VSP-300 (Biologic) electrochemical workstation. The working electrodes were fabricated by following method: firstly, 5 mg of photocatalyst was ultrasonically dispersed in the solution containing 0.5 mL of ethanol and 10 µL Nafion. After 3 h ultrasonication, the mixture was dropped and spread on a half of indium tin oxide (ITO) glass (20×10 mm). Subsequently, the as-prepared working electrodes were dried at 150 °C for 6 h. The counter and reference electrode were served by platinum sheet and Ag/AgCl, respectively. 0.1 M Na<sub>2</sub>SO<sub>4</sub> aqueous solution was used as electrolyte. A 300 W Xenon lamp (Aulight) coupled with a UV cutoff filter ( $\lambda > 420$  nm) was applied as the light source. Electrochemical impedance

spectroscopy (EIS) spectra were obtained in the frequency range of  $10^{-1}$ - $10^5$  Hz. MottSchottky plots were recorded on 500, 1000, and 1500 Hz frequencies.

### Density functional theory calculations

All Spin-polarization density functional theory (DFT) calculations was employed through the first-principles<sup>1, 2</sup> using the Perdew-Burke-Ernzerhof (PBE)<sup>3</sup> formulation within the generalized gradient approximation (GGA). The projected augmented wave (PAW) potentials<sup>4, 5</sup> are chosen to describe the ionic cores, and a plane wave basis set with a kinetic energy cutoff of 450 eV was used to account for the valence electrons. Van der Waals interactions have been considered using the DFT-D3 method of Grimme.<sup>6, 7</sup> The electronic energy and geometry optimization were considered self-consistent and convergent when the energy change was smaller than  $10^{-5}$  eV and 0.02 eV Å<sup>-1</sup>, respectively. The Brillouin zone with a  $2\times2\times1$  Gamma-centered grid was used during the relaxation. The 13 Å vacuum layer was normally added to the surface to eliminate the artificial interactions between periodic images. Spin-polarized calculations were executed for this calculation.

For each elementary step, the Gibbs reaction free energy  $\Delta G$  is defined as the difference between free energies of the initial and final states and is given by the following expression:

$$\Delta G = \Delta E + \Delta ZPE - T\Delta S$$

where  $\Delta E$  is the reaction energy of reactant and product molecules adsorbed on the catalyst surface, obtained from DFT calculations;  $\Delta ZPE$  and  $\Delta S$  are the change in zero-point energies and entropy because of the reaction.

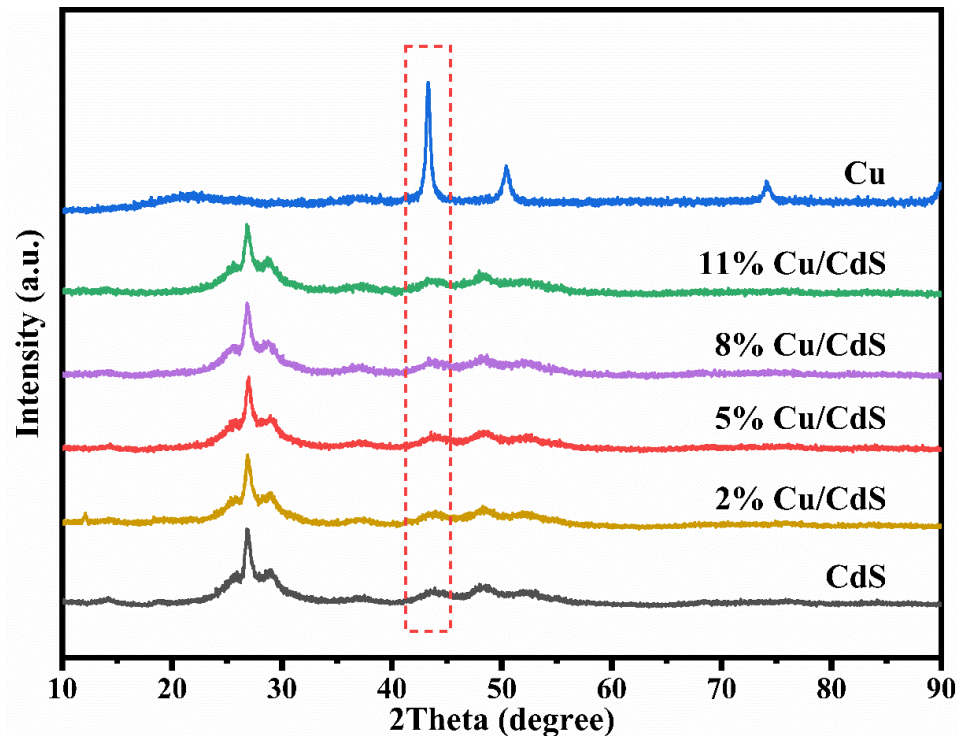


**Fig. S1** XRD patterns of Cu/CdS.

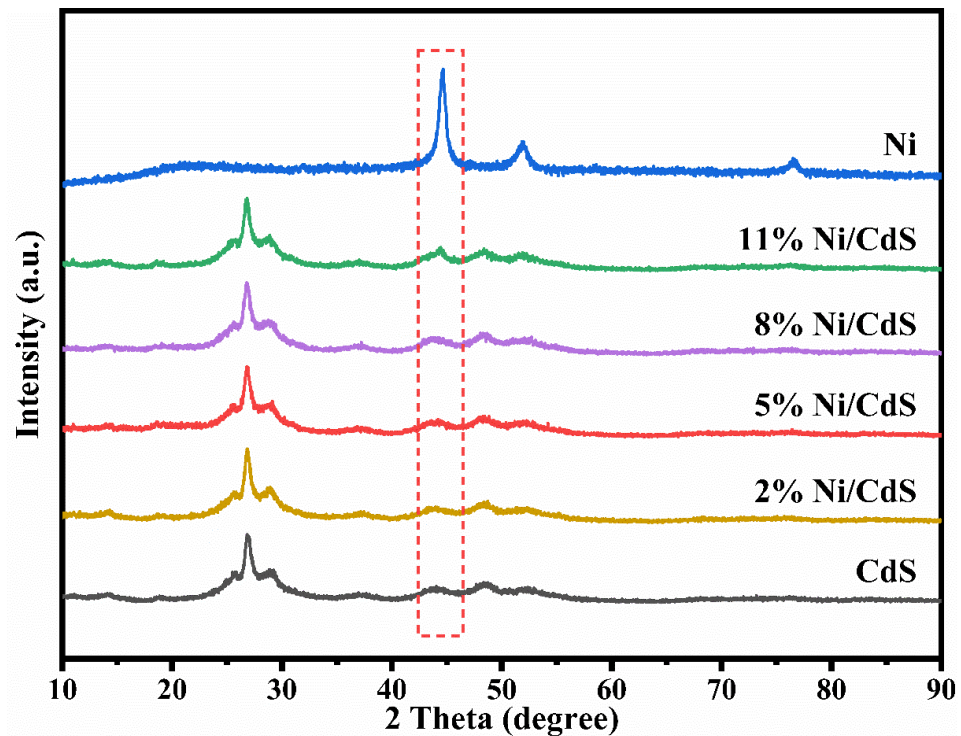


**Fig. S2** XRD patterns of Ni/CdS.

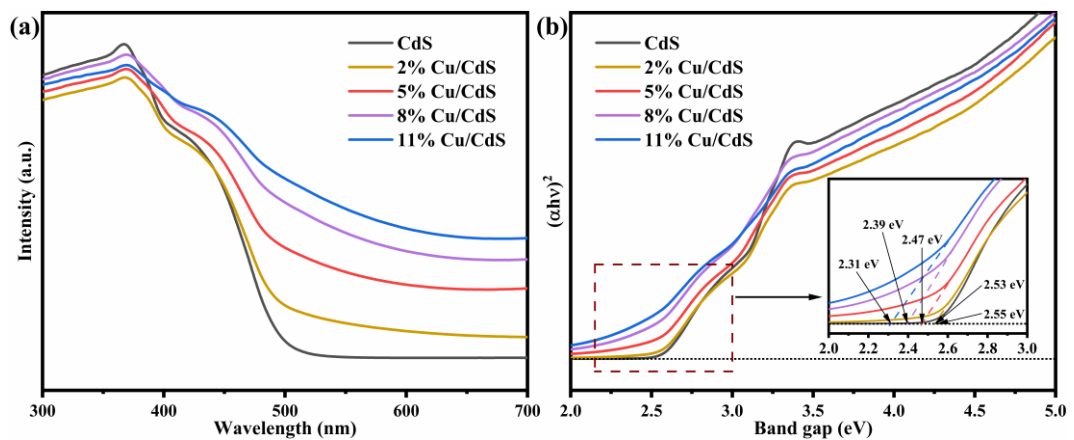


**Fig. S3** (a) UV-vis spectra and (b) Tauc plot of Cu/CdS.

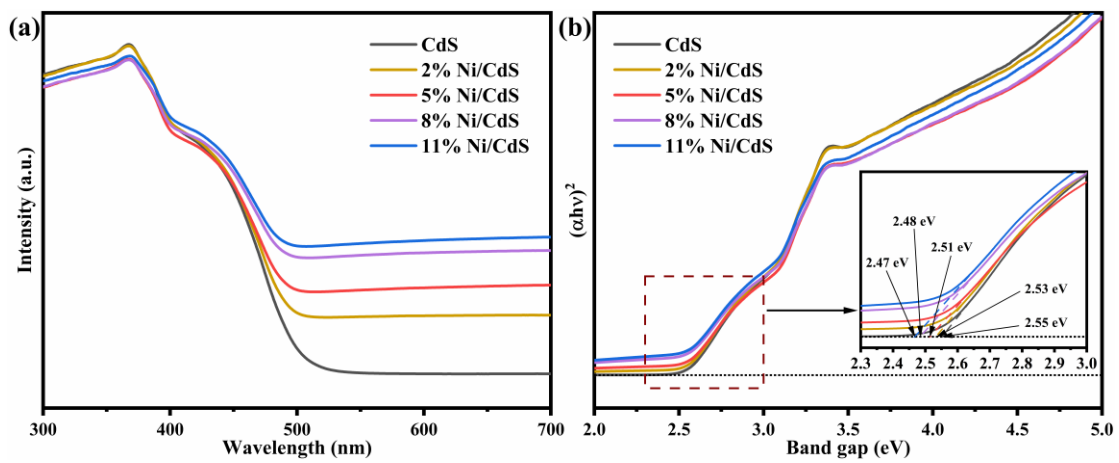


**Fig. S4** (a) UV-vis spectra and (b) Tauc plot of Ni/CdS.

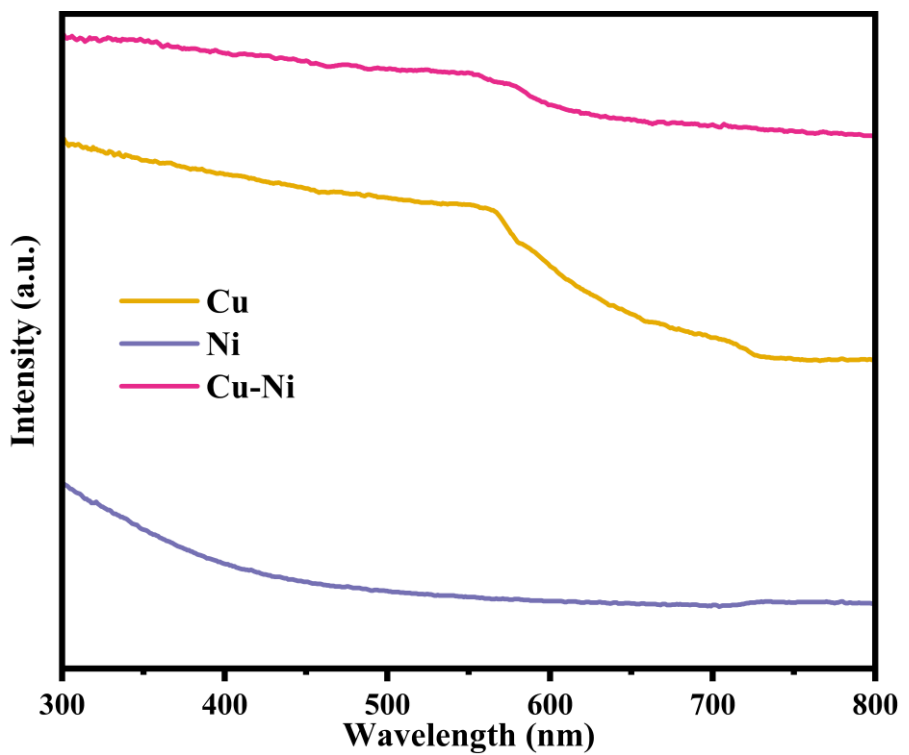


**Fig. S5** UV-vis spectra of Cu, Ni, and Cu-Ni samples.

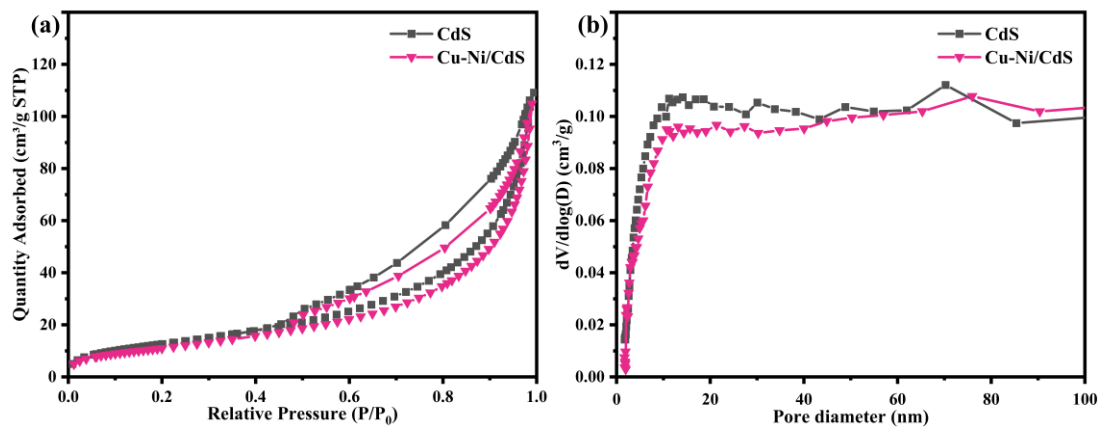


**Fig. S6** (a) N<sub>2</sub> adsorption-desorption isotherms and (b) pore-size distribution curves of CdS and Cu-Ni/CdS samples.

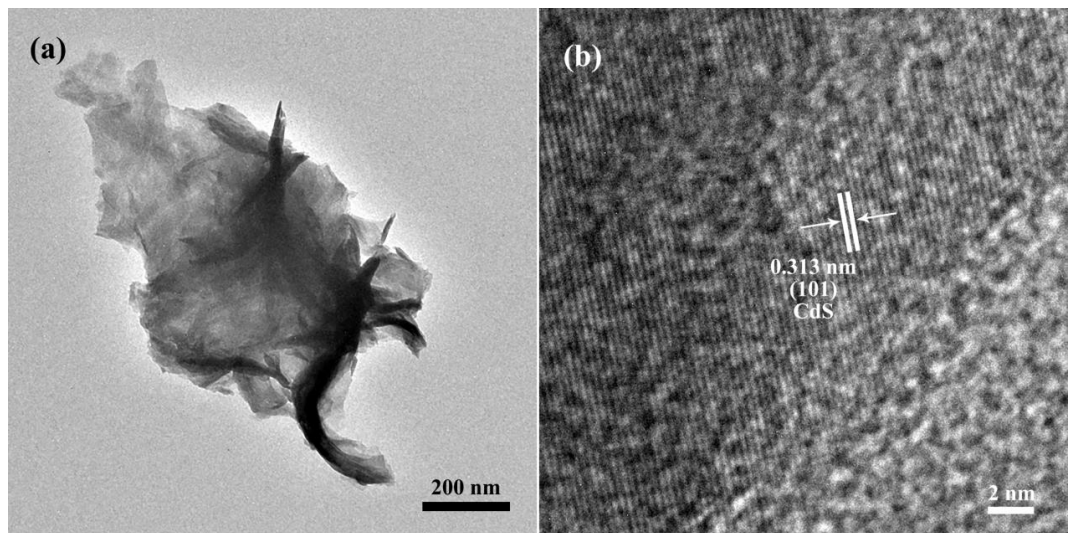


**Fig. S7**(a) TEM image and (b) HRTEM of pure CdS.

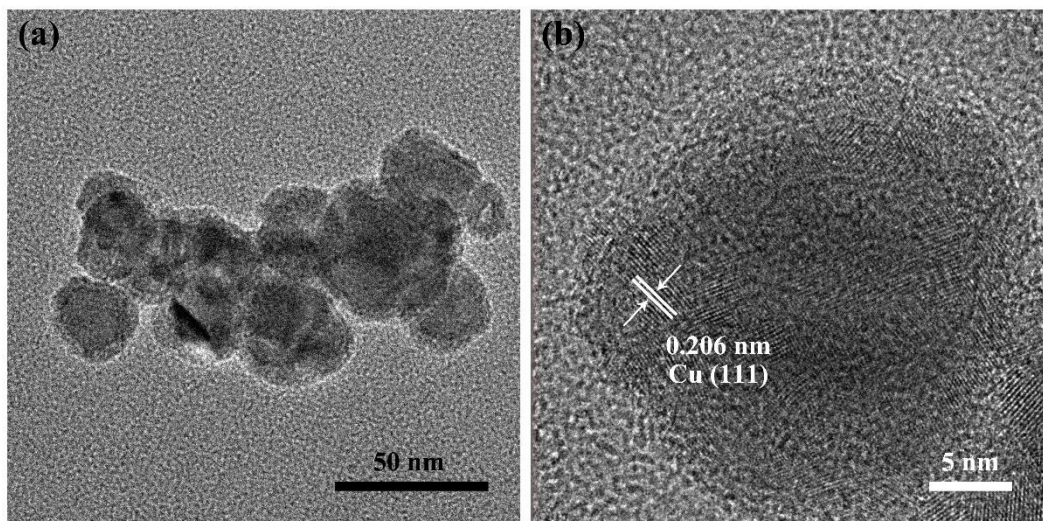


**Fig. S8** (a) TEM image and (b) HRTEM of pure Cu nanoparticles.

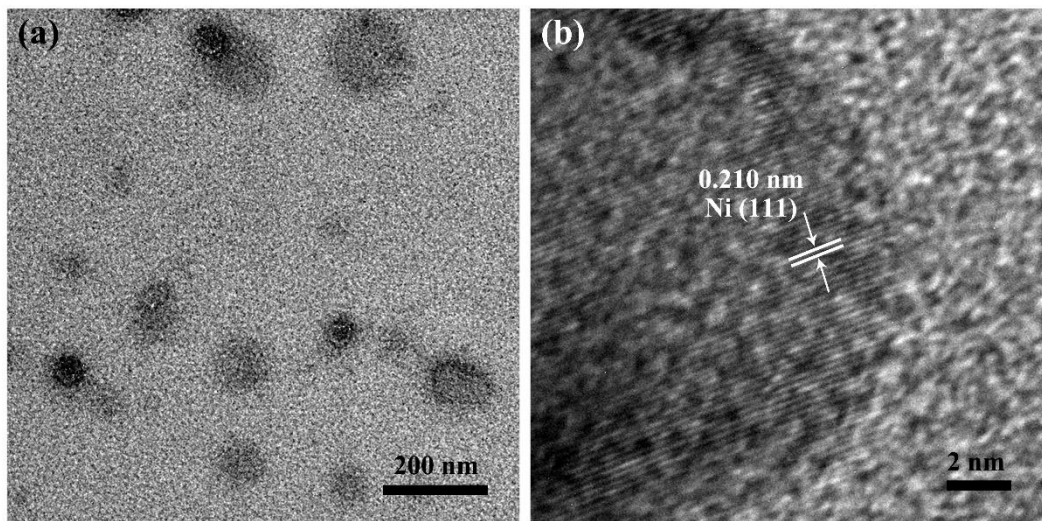


**Fig. S9** (a) TEM image and (b) HRTEM of pure Ni nanoparticles.

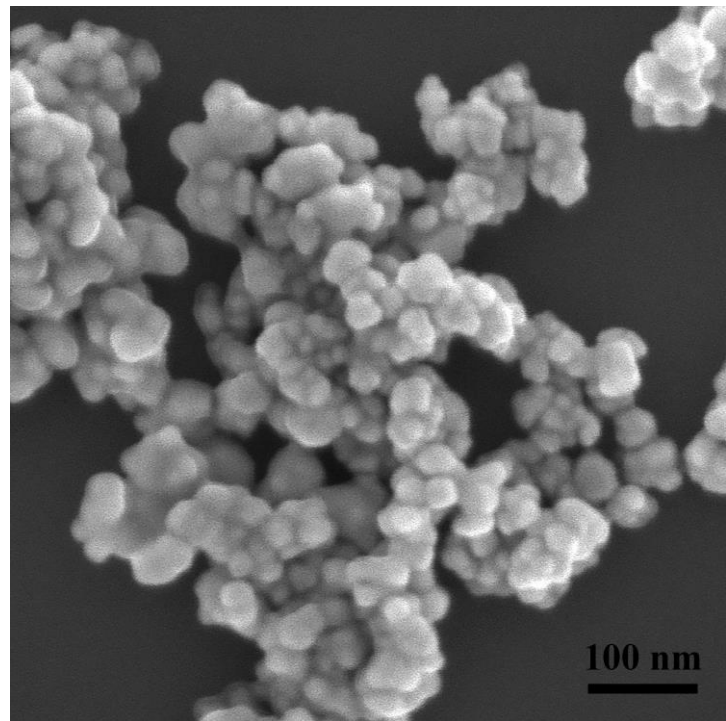


**Fig. S10** SEM image of Cu-Ni nanoparticles.

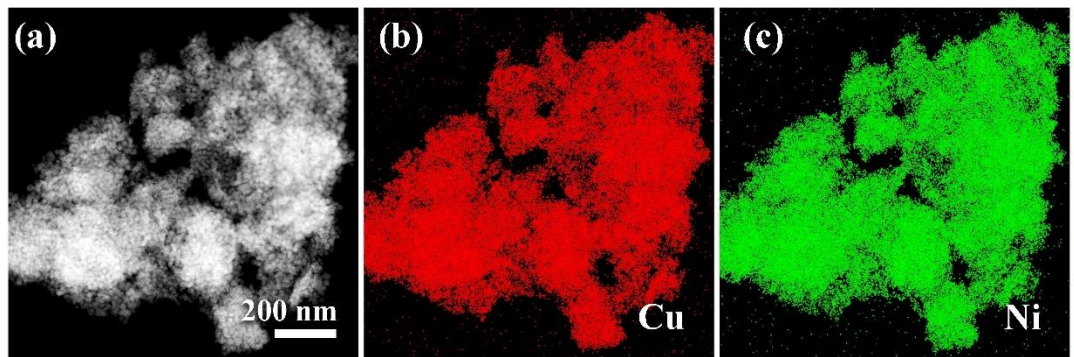


**Fig. S11** EDS elemental mapping images of Cu-Ni nanoparticles.

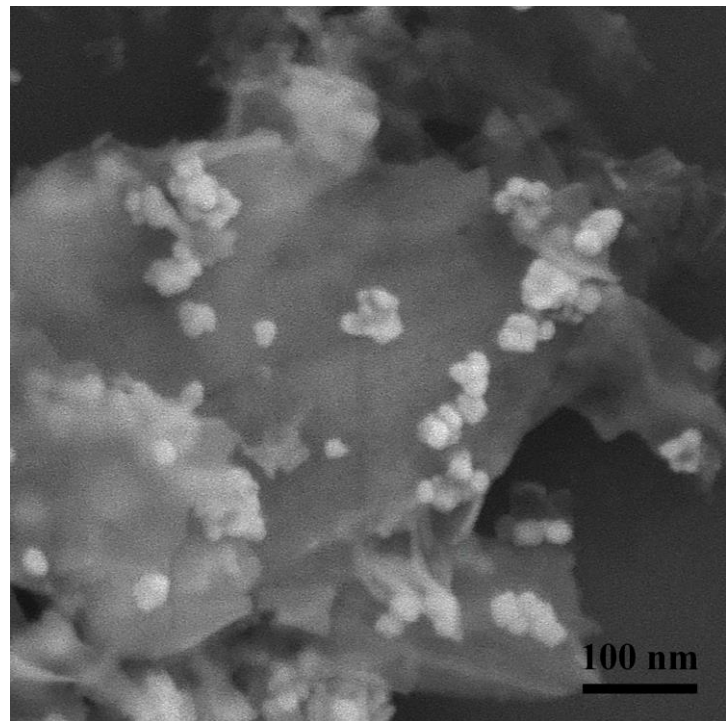


**Fig. S12** SEM image of 8% Cu-Ni/CdS nanocomposite.

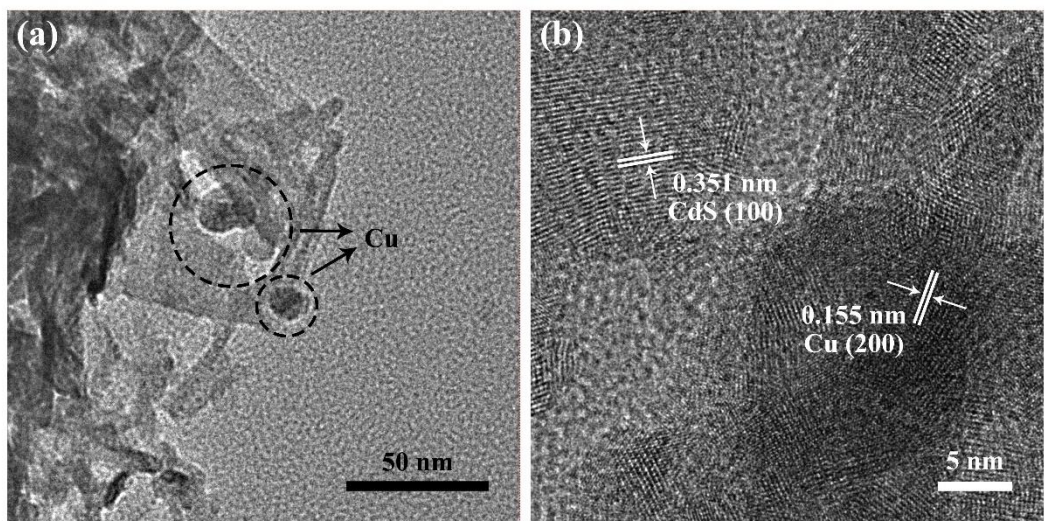


**Fig. S13** (a) TEM image and (b) HRTEM of Cu/CdS nanocomposite.

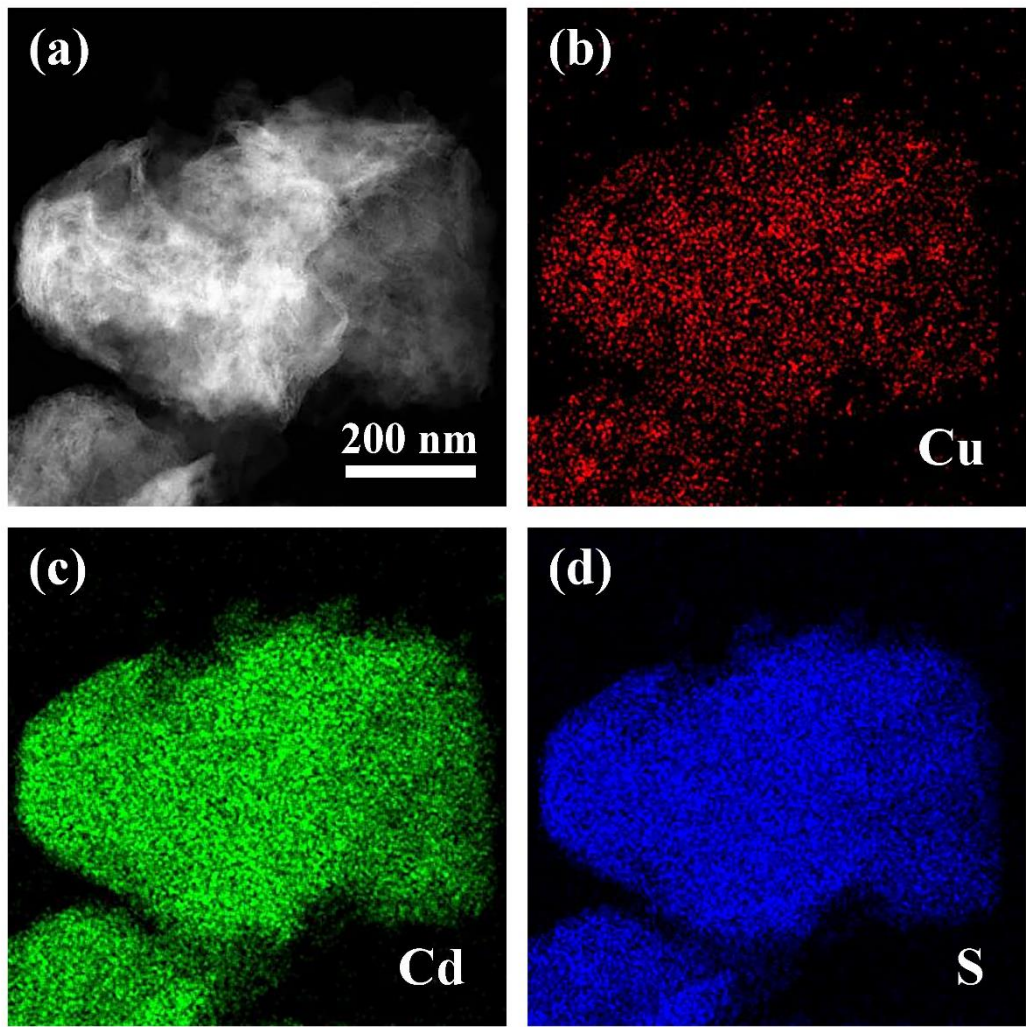


**Fig. S14** EDS elemental mapping images of Cu/CdS nanocomposite.

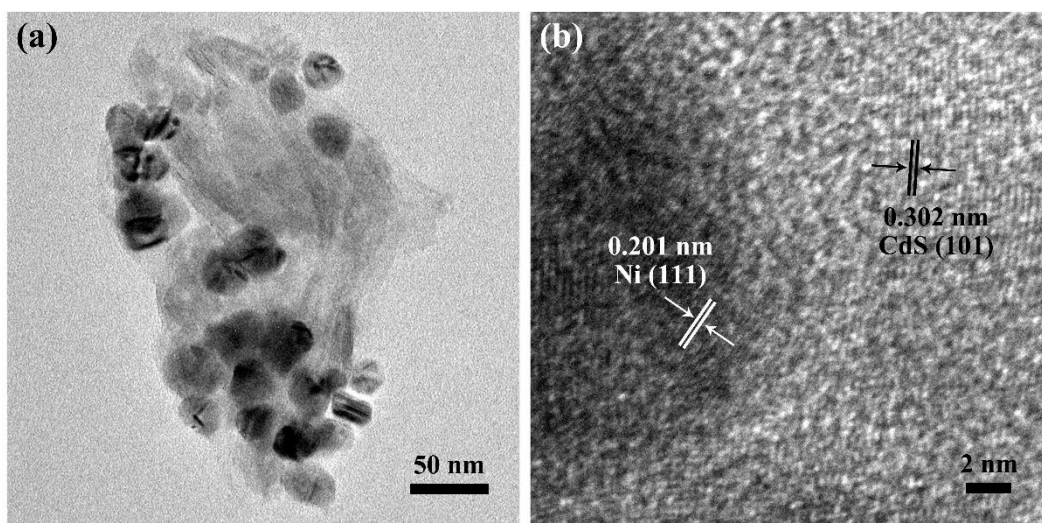


**Fig. S15** (a) TEM image and (b) HRTEM of Ni/CdS nanocomposite.

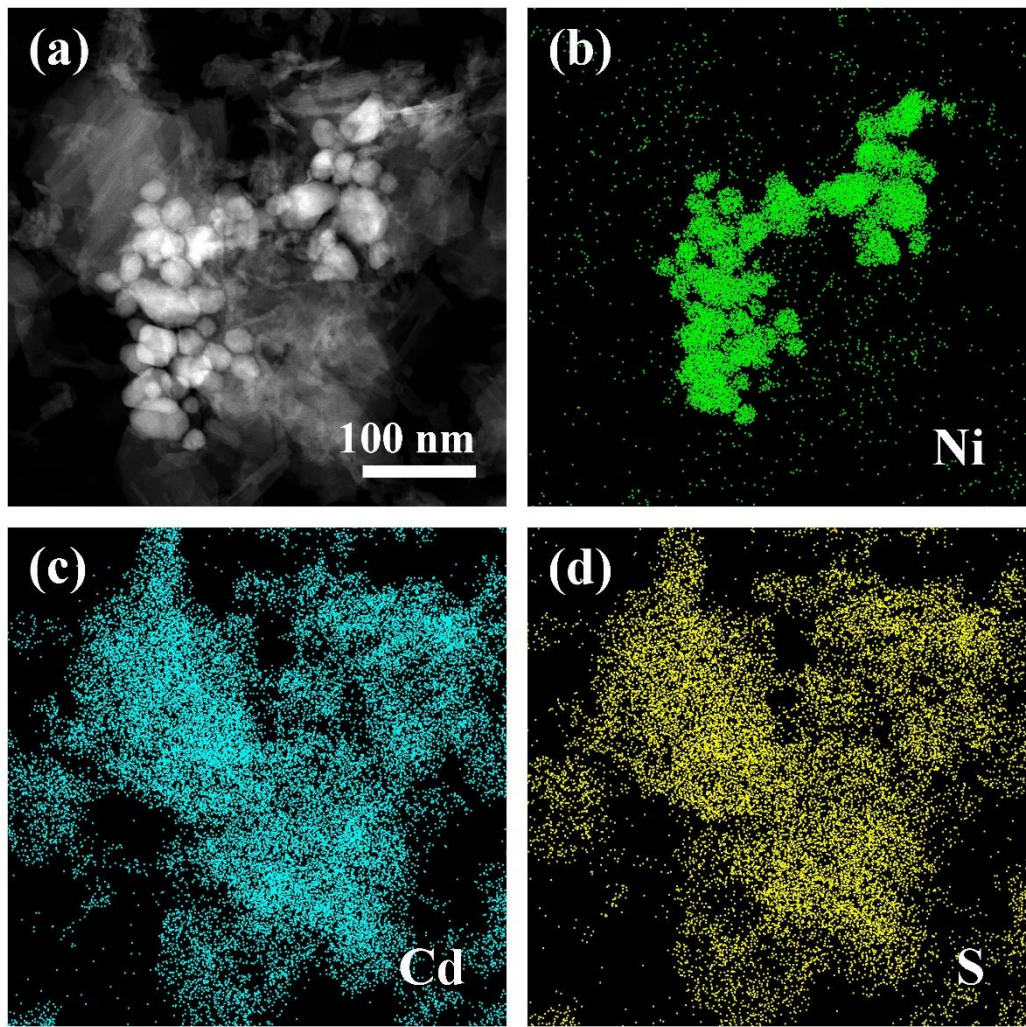


**Fig. S16** EDS elemental mapping images of Ni/CdS nanocomposite.

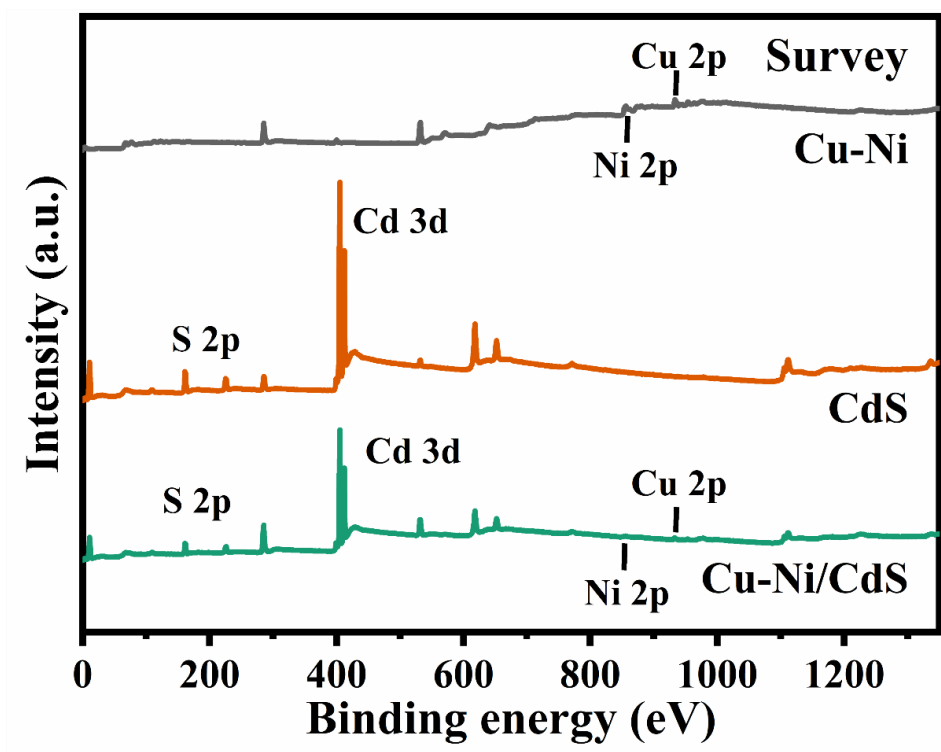


**Fig. S17** (a) XPS survey spectra of CdS, Cu-Ni and 8% Cu-Ni/CdS.

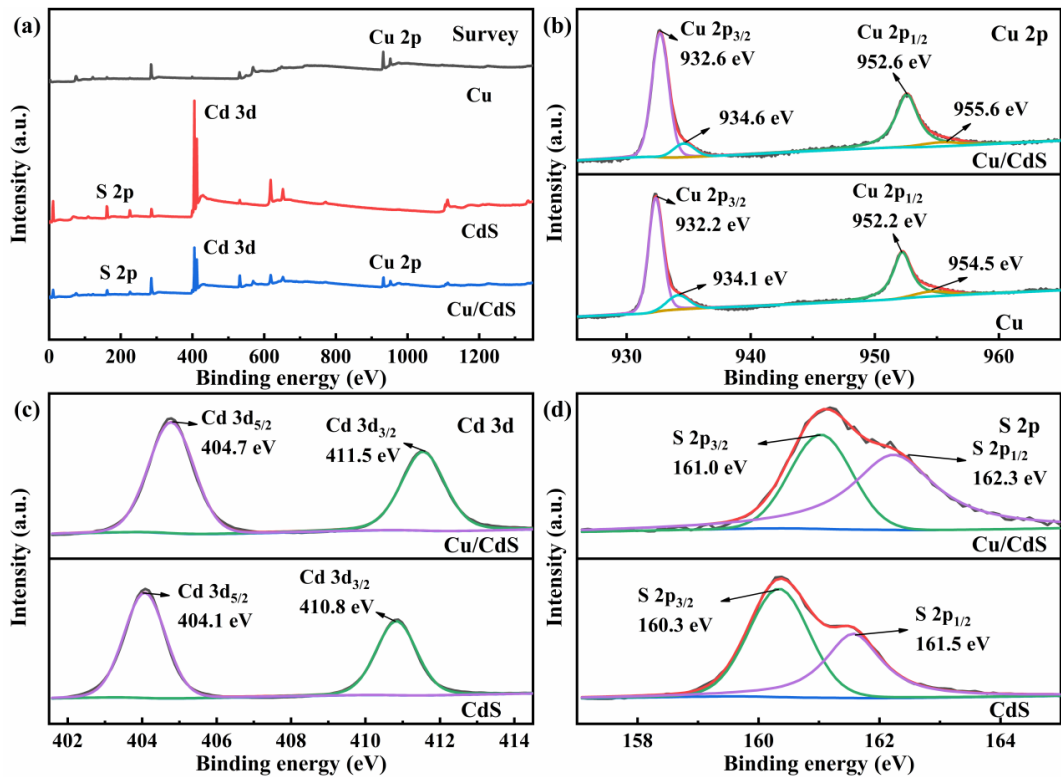


**Fig. S18** (a) XPS survey spectra of CdS, Cu and 5% Cu/CdS. High-resolution XPS spectra of (b) Cu 2p, (c) Cd 3d and (d) S 2p of CdS, Cu and 5% Cu/CdS.

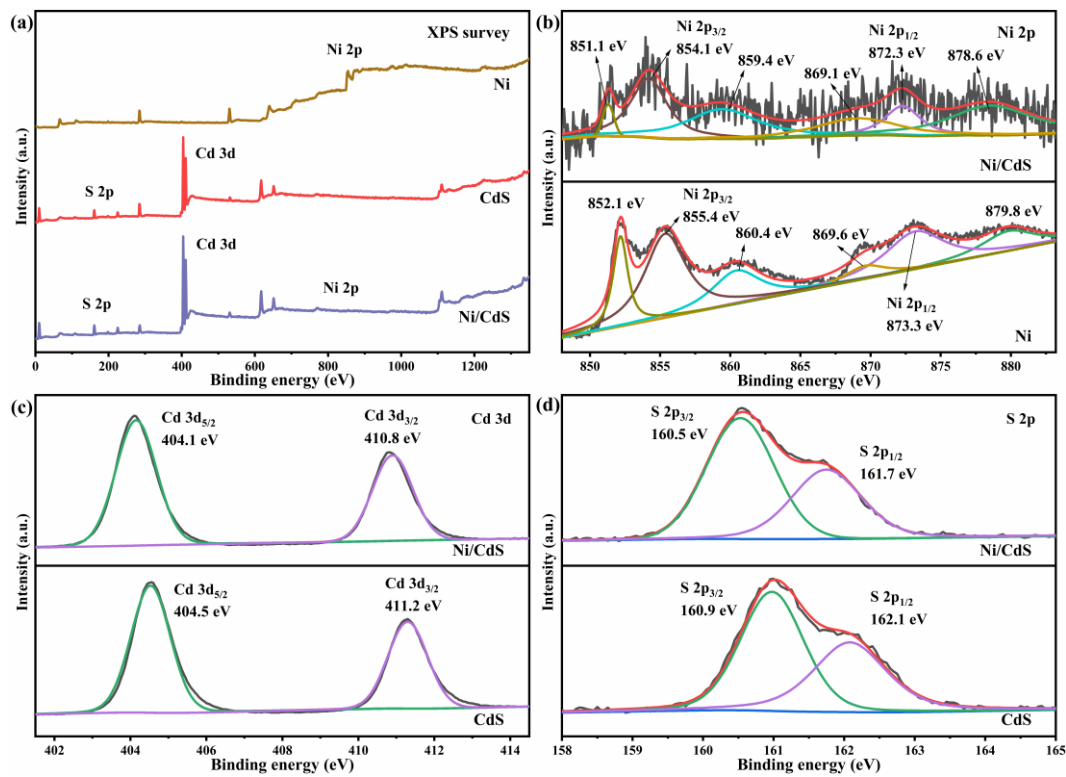


**Fig. S19** (a) XPS survey spectra of CdS, Ni and 5% Ni/CdS. High-resolution XPS spectra of (b) Ni 2p, (c) Cd 3d and (d) S 2p of CdS, Ni and 5% Ni/CdS.

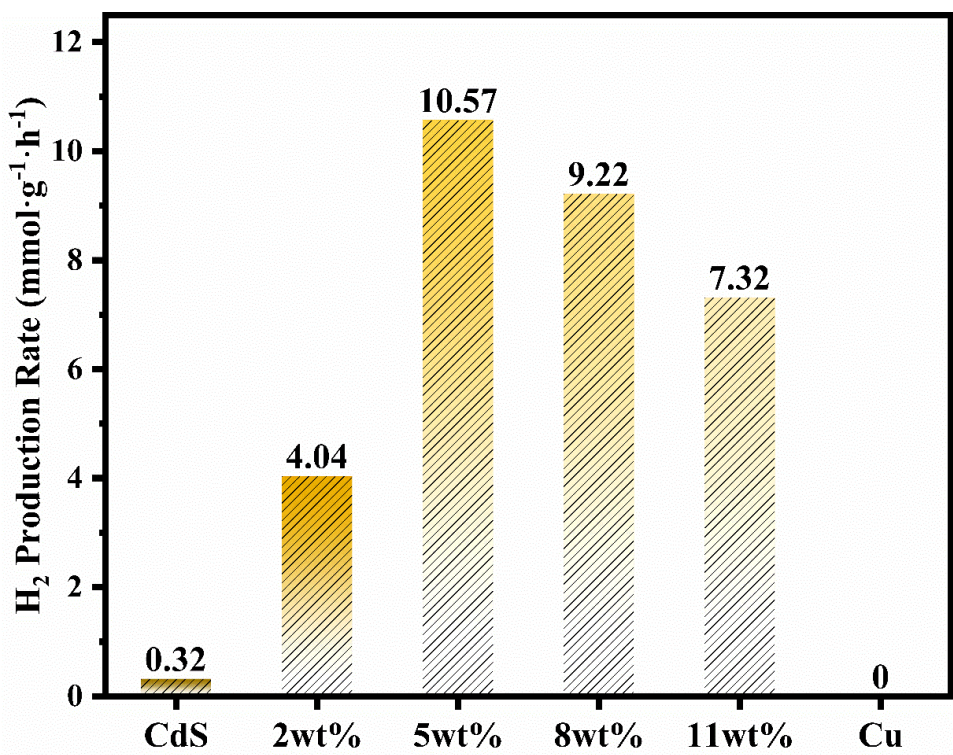


**Fig. S20** Photocatalytic  $\text{H}_2$  generation rate of different Cu loading in Cu/CdS.

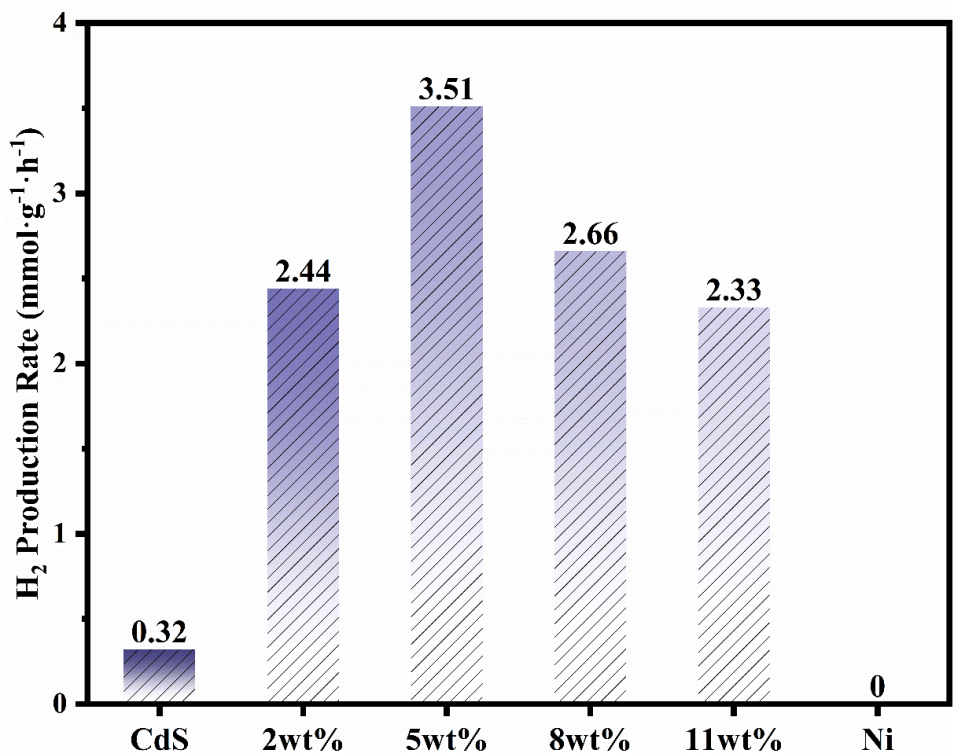


**Fig. S21** Photocatalytic  $\text{H}_2$  generation rate of different Ni loading in Ni/CdS.

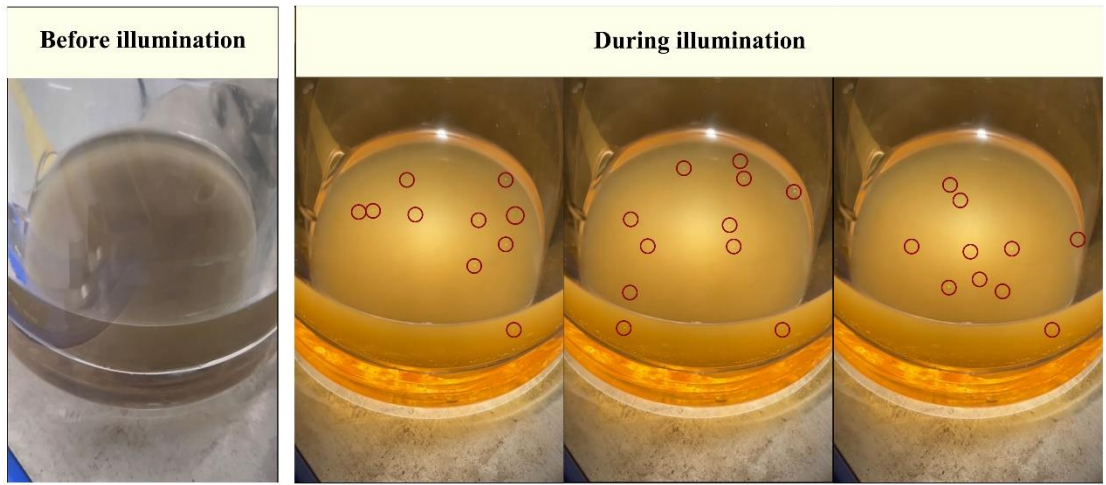


**Fig. S22** Real-time photos of H<sub>2</sub> production (the red circles represent the position of H<sub>2</sub> bubbles).

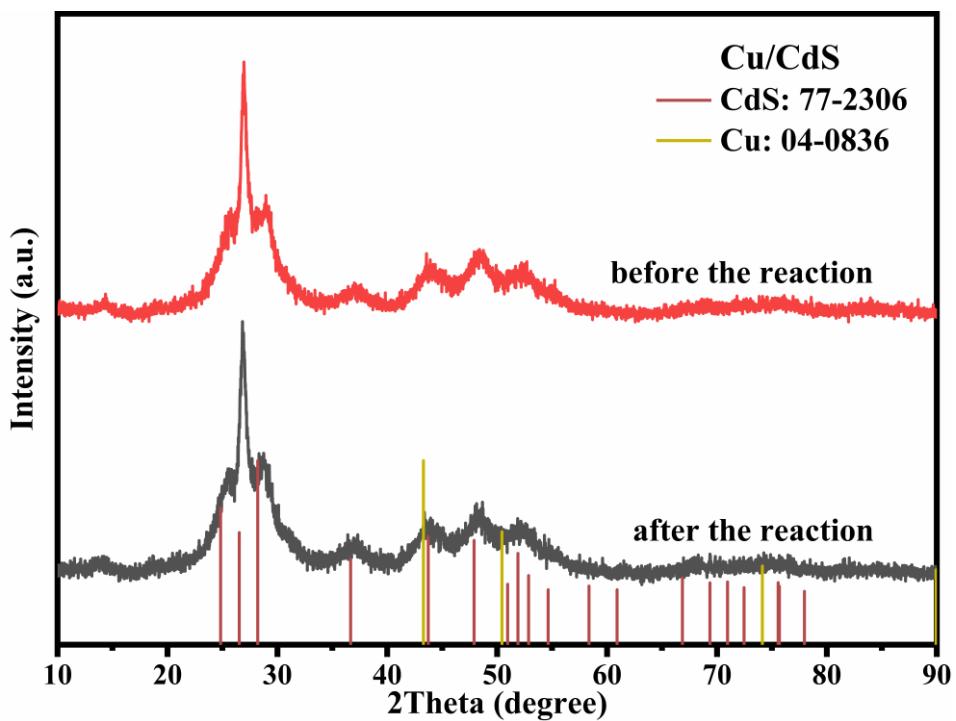


**Fig. S23** XRD pattern of Cu/CdS before and after cycling run.

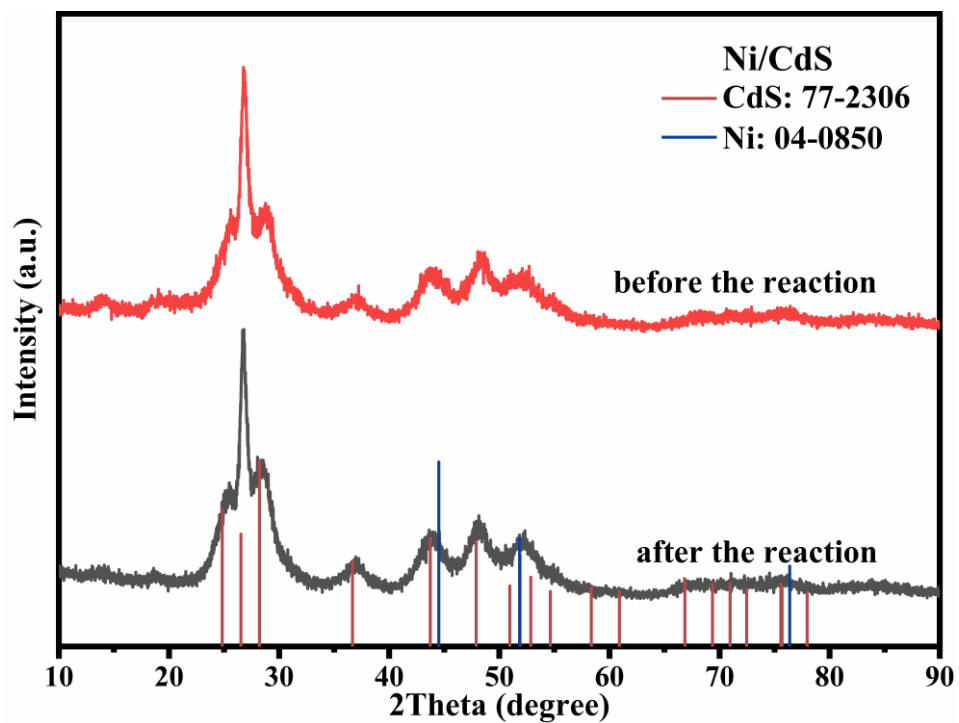


**Fig. S24** XRD pattern of Ni/CdS before and after cycling run.

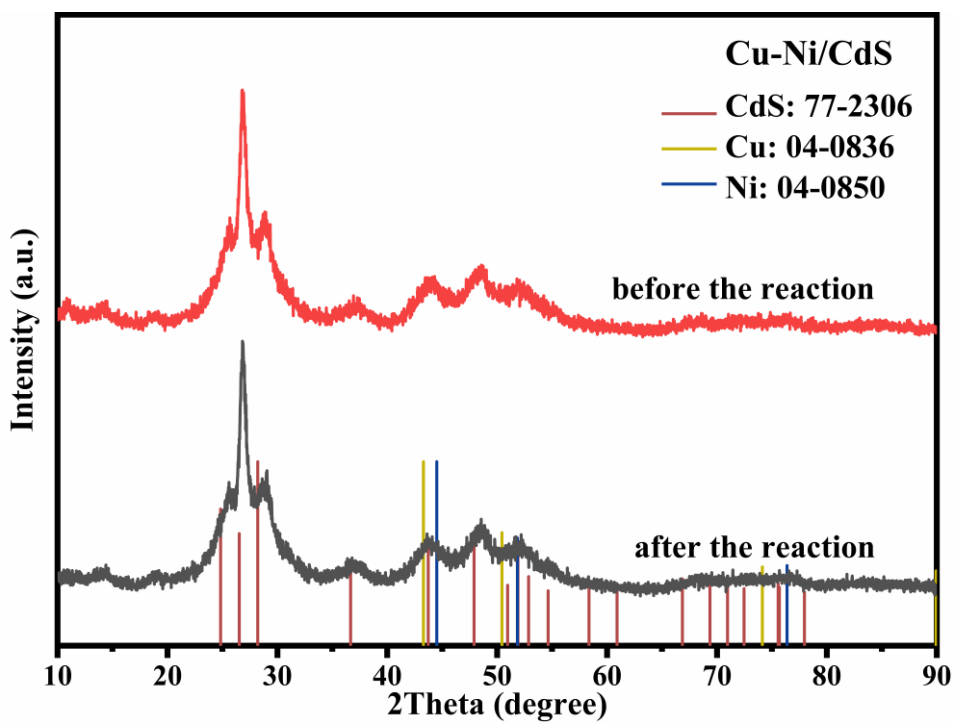


**Fig. S25** XRD pattern of Cu-Ni/CdS before and after cycling run.

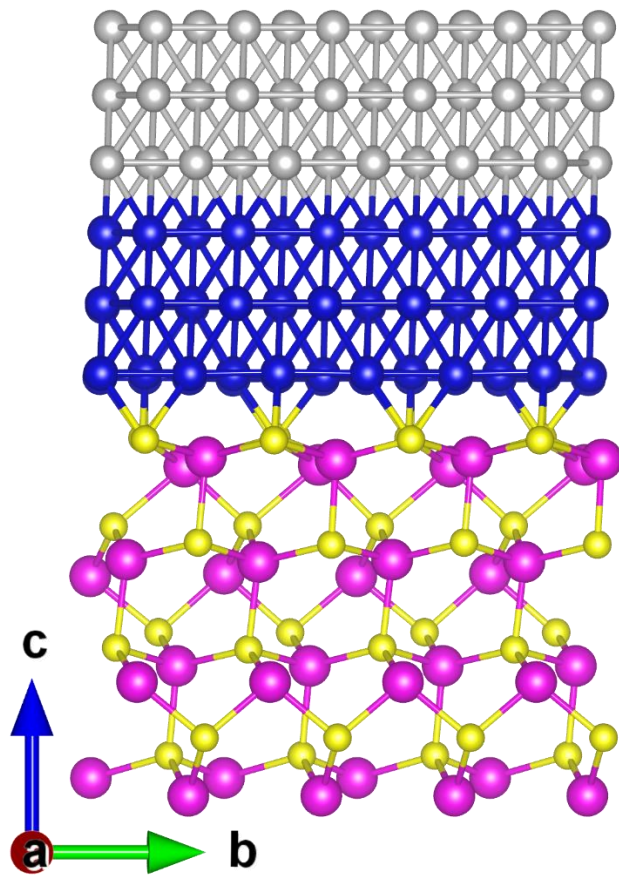


**Fig. S26** The DFT optimization models of Cu-Ni/CdS. (Cd: pink spheres, S: yellow spheres, Cu: dark blue spheres, Ni: light gray spheres).

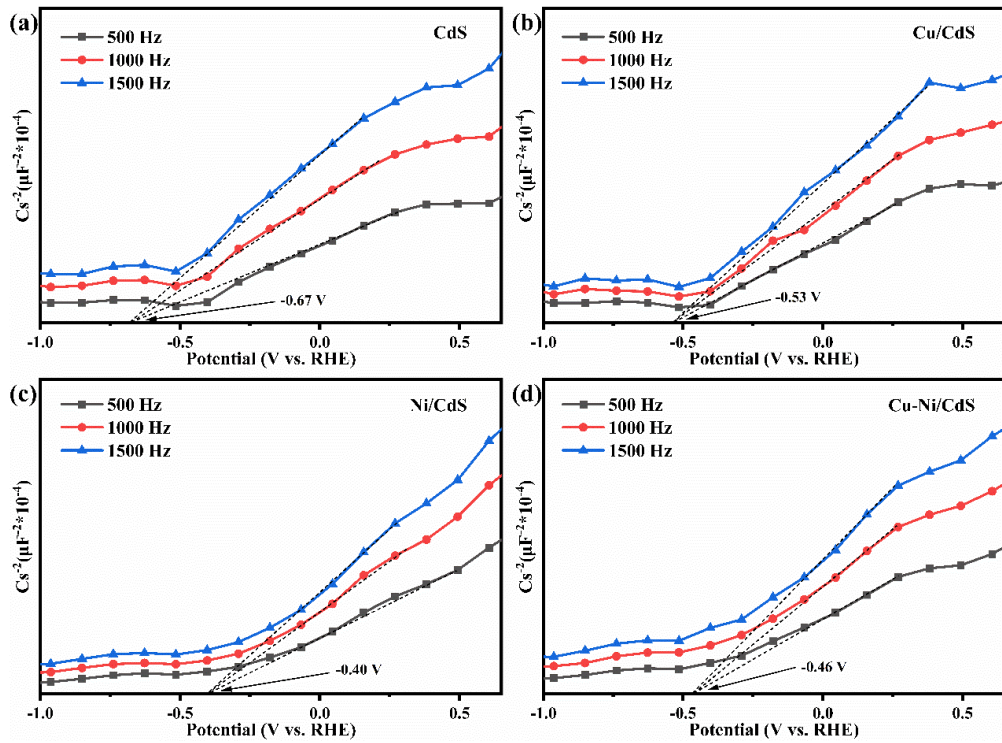


**Fig. S27** Mott-Schottky plots of (a) CdS, (b) Cu/CdS, (c) Ni/CdS and (d) Cu-Ni/CdS.

**Table S1.** The concentration of Cu and Ni in Cu-Ni and 8% Cu-Ni/CdS samples.

photocatalyst	Measured concentration (mg·L <sup>-1</sup> )		Molecular weight (mol)		Mole ratio (Cu:Ni)
	Cu	Ni	Cu	Ni	
<b>Cu-Ni</b>	25.309	22.043	0.0398	0.0376	1.06
<b>8% Cu-Ni/CdS</b>	2.410	2.177	0.0038	0.0037	1.02

**Table S2.** BET surface area, mean pore diameter and pore volume of CdS and 8% Cu-Ni/CdS samples.

<b>photocatalyst</b>	<b>S<sub>BET</sub></b> <b>(m<sup>2</sup>·g<sup>-1</sup>)</b>	<b>Average pore diameter (nm)</b>	<b>Pore volume (cm<sup>3</sup>·g<sup>-1</sup>)</b>
<b>CdS</b>	48.19	13.93	0.1678
<b>8% Cu-Ni/CdS</b>	41.96	15.47	0.1622

**Table S3.** Photocatalytic H<sub>2</sub> evolution activity of CdS-based photocatalysts.

Photocatalyst	Additives	Light source	Scavenger	Activity (mmol·h <sup>-1</sup> ·g <sup>-1</sup> )	Refs
CdS	CoO <sub>x</sub>	420 W Xe lamp (λ> 420 nm)	Na <sub>2</sub> S/Na <sub>2</sub> SO <sub>3</sub>	3.500	<sup>8</sup>
CdS	Co <sub>9</sub> S <sub>8</sub>	300 W Xe lamp Simulated sunlight	Na <sub>2</sub> S/Na <sub>2</sub> SO <sub>3</sub>	1.061	<sup>9</sup>
CdS	MoO <sub>x</sub> S <sub>y</sub>	300 W Xe lamp (λ> 420 nm)	methanol	1.756	<sup>10</sup>
CdS	F/G	300 W Xe lamp (λ>420 nm)	methanol	0.127	<sup>11</sup>
CdS	GNR	300 W Xe lamp (λ>400 nm)	Lactic acid	1.890	<sup>12</sup>
CdS	g-C <sub>3</sub> N <sub>4</sub>	300W Xe lamp Simulated sunlight	Lactic acid	3.370	<sup>13</sup>
CdS	Cu <sub>2</sub> Ni <sub>1</sub>	100 W broad band lamp	ethanol	14.160	<sup>14</sup>
CdS	ZnO	350W Xe lamp	Na <sub>2</sub> S/Na <sub>2</sub> SO <sub>3</sub>	4.134	<sup>15</sup>
CdS	Ca@CoP <sub>x</sub>	300 W Xe lamp (λ>420 nm)	Na <sub>2</sub> S/Na <sub>2</sub> SO <sub>3</sub>	2.442	<sup>16</sup>
CdS	Mo <sub>2</sub> C	Xe lamp (λ>420 nm)	Lactic acid	7.700	<sup>17</sup>
CdS	Ru/WC	300 W Xe lamp (λ>420 nm)	Lactic acid	16.800	<sup>18</sup>
CdS	Ti <sub>3</sub> C <sub>2</sub> /MoS <sub>2</sub>	300 W Xe lamp (λ>420 nm)	Lactic acid	14.88	<sup>19</sup>
CdS	VC	300 W Xe lamp (λ>420 nm)	Lactic acid	14.2	<sup>20</sup>
CdS	Ni <sub>2</sub> P	300 W Xe lamp (λ>420 nm)	Lactic acid	18.2	<sup>21</sup>
CdS	Ni <sub>3</sub> C	300 W Xe lamp (λ>420 nm)	Na <sub>2</sub> S/Na <sub>2</sub> SO <sub>3</sub>	14.28	<sup>22</sup>
<b>CdS</b>	<b>Cu-Ni</b>	<b>300 W Xe lamp (λ&gt; 420 nm)</b>	<b>Na<sub>2</sub>S/Na<sub>2</sub>SO<sub>3</sub></b>	<b>28.19</b>	<b>This work</b>

**Table S4.** AQY of 8% Cu-Ni/CdS under different wavelength light.

<b>Light wavelength (nm)</b>	<b>Photocatalytic H<sub>2</sub> evolution rate (mmol·h<sup>-1</sup>·g<sup>-1</sup>)</b>	<b>AQY (%)</b>
<b>400</b>	5.36	21.5
<b>420</b>	2.72	10.8
<b>435</b>	2.76	11.6
<b>450</b>	3.55	13.5
<b>475</b>	4.36	12.6
<b>500</b>	3.84	12.7
<b>520</b>	3.55	12.1
<b>550</b>	1.72	5.6
<b>600</b>	0.67	5.3
<b>650</b>	0.23	1.7
<b>700</b>	0.15	0.7

**Table S5.** E<sub>g</sub>, CB and VB of CdS, 5% Cu/CdS, 5% Ni/CdS and 8% Cu-Ni/CdS.

photocatalyst	E <sub>g</sub> (V)	CB (V)	VB (V)
<b>CdS</b>	2.55	-0.67	1.88
<b>5% Cu/CdS</b>	2.47	-0.53	1.94
<b>5% Ni/CdS</b>	2.51	-0.40	2.11
<b>8% Cu-Ni/CdS</b>	2.48	-0.46	2.02

## References

1. K. G and F. J., *Comp. Mater. Sci.*, 1996, **6**, 15-50.
2. K. G and F. J., *Phys. Rev. B*, 1996, **54**, 11169.
3. P. J. P. B. K and E. M., *Phys. Rev. Lett.*, 1996, **77**, 3865.
4. G. Kresse and D. Joubert, *Phys. Rev. B*, 1999, **59**, 1758.
5. P. E. Blöchl, *Phys. Rev. B*, 1994, **50**, 17953-17979.
6. S. Grimme, J. Antony, S. Ehrlich and H. Krieg, *J. Chem. Phys.*, 2010, **132**, 154104.
7. S. Grimme, S. Ehrlich and L. Goerigk, *J. Comput. Chem.*, 2011, **32**, 1456-1465.
8. Y. Liu, S. Ding, Y. Shi, X. Liu, Z. Wu, Q. Jiang, T. Zhou, N. Liu and J. Hu, *Appl. Catal. B*, 2018, **234**, 109-116.
9. B. Qiu, Q. Zhu, M. Du, L. Fan, M. Xing and J. Zhang, *Angew. Chem. Int. Edit.*, 2017, **56**, 2684-2688.
10. X. Lu, C. Y. Toe, F. Ji, W. Chen, X. Wen, R. J. Wong, J. Seidel, J. Scott, J. N. Hart and Y. H. Ng, *ACS Appl. Mater.*, 2020, **12**, 8324-8332.
11. W. Wang, Y. Tao, J. Fan, Z. Yan, H. Shang, D. L. Phillips, M. Chen and G. Li, *Adv. Funct. Mater.*, 2022, **32**, 2201357.
12. Y. Xia, B. Cheng, J. Fan, J. Yu and G. Liu, *Small*, 2019, **15**, 1902459.
13. Y. Ran, Y. Cui, Y. Zhang, Y. Fang, W. Zhang, X. Yu, H. Lan and X. An, *Chem. Eng. J.*, 2022, **431**, 133348.
14. F. Saleem, M. Z. Abid, K. Rafiq, A. Rauf, K. Ahmad, S. Iqbal, R. Jin and E. Hussain, *Int. J. Hydrot. Energy*, 2024, **52**, 305-319.
15. S. Wang, B. Zhu, M. Liu, L. Zhang, J. Yu and M. Zhou, *Appl. Catal. B*, 2019, **243**, 19-26.
16. X. Ren, F. Liu, Q. Wang, H. Song, S. Luo, S. Li, G. Yang, B. Deng, Z. Huang, X.-S. Wang, L. Shi and J. Ye, *Appl. Catal. B*, 2022, **303**, 120887.
17. D. Ruan, M. Fujitsuka and T. Majima, *Appl. Catal. B*, 2020, **264**, 118541.
18. K. Lin, L. Feng, D. Li, J. Zhang, W. Wang and B. Ma, *Appl. Catal. B*, 2021, **286**, 119880.
19. C. Wu, W. Huang, H. Liu, K. Lv and Q. Li, *Appl. Catal. B*, 2023, **330**, 122653.
20. L. Tian, S. Min and F. Wang, *Appl. Catal. B*, 2019, **259**, 118029.
21. Z. Wang, Z. Qi, X. Fan, D. Y. C. Leung, J. Long, Z. Zhang, T. Miao, S. Meng, S. Chen and X. Fu, *Appl. Catal. B*, 2021, **281**, 119443.
22. S. Ma, Y. Deng, J. Xie, K. He, W. Liu, X. Chen and X. Li, *Appl. Catal. B*, 2018, **227**, 218-228.